Magnetic Resonance Imaging and Cross-Sectional Anatomy of the Coelomic Cavity in a Red-Eared Slider (*Trachemys scripta elegans*) and Yellow-Bellied Sliders (*Trachemys scripta scripta*)

Noémie M. Summa[1,2], DVM, Emmanuel E. Risi[3], DVM, Marion Fusellier[1], DVM, David Sanchez-Migallon Guzman[2], LV, MS, DECZM (Avian), DACZM, Allison L. Zwingenberger[2], DVM, DACVR, DECVDI, MAS, Stephane Madec[1], Christian Raphaël[1], Eric R.P. Betti[1], DMV, Msc.

1. Centre Hospitalier Universitaire Vétérinaire, Ecole Nationale Vétérinaire de Nantes, ONIRIS, 44307 Nantes, France

2. School of Veterinary Medicine, University of California-Davis, Davis, CA 95616, USA

3. Centre Hospitalier Vétérinaire Altantia, Nantes, France

This manuscript represents a portion of a thesis submitted by Dr. Noémie Summa to the National Veterinary School of Nantes as partial fulfillment of the requirements for her doctorate.

Abstract: The aim of this study was to determine the normal coelomic structures of a healthy red-eared slider (*Trachemys scripta elegans*) and yellow-bellied sliders (*Trachemys scripta scripta*) using magnetic resonance images and gross cross-sectional anatomy. Three- or six-centimeter thick, T1-weighted and T2-weighted images were obtained from three live adult red-eared ($n = 1$) and yellow-bellied sliders ($n = 2$) with a 1-Tesla superconducting magnet and a surface coil. Magnetic resonance imaging was performed in transverse, sagittal, and dorsal planes. Images of the coelomic cavity were compared to frozen, cross-sectional cadaveric anatomy of the same turtles. Anatomic structures were identified and labeled. Resulting images presented excellent, detailed information of coelomic structures. The intent of this study was to develop an atlas of cross-sectional anatomy and magnetic resonance appearance of the normal coelomic cavity in red-eared and yellow-bellied sliders that can be used as a reference for the interpretation of any cross-sectional modality.

Key Words: Anatomy, chelonian, imaging, magnetic resonance, *Trachemys scripta*, turtle

Introduction

Because of vague clinical signs and the limits of physical examination in turtles, tortoises, and terrapins, complementary diagnostic procedures are often needed. Diagnostic imaging modalities such as ultrasound or radiography for evaluation of coelomic structures are limited by the presence of the shell. In contrast, the quality of magnetic resonance (MR) imaging is not affected by the shell and MR imaging provides excellent details of soft tissue structures.

Few reports concerning the use of MR imaging in chelonians have been published. The MR appearance of coelomic structures has been described in the spur-thighed tortoise (*Testudo graeca*) (Straub and Jurina, 2001; Wilkinson *et al.*, 2004), Aldabra giant tortoise (*Dipsochelys elephantina*) (Wilkinson *et al.*, 2004), Hermann's tortoise (*Testudo hermanni*) (Straub and Jurina, 2001), leopard tortoise (*Geochelone pardalis pardalis*) (Raiti and Haramati, 1997), central Asian tortoise (*Testudo horsfieldii*) (Silverman and Janssen, 2006), loggerhead sea turtle (*Caretta caretta*) (Valente *et al.*, 2006), green turtle (*Chelonia mydas*) (Croft *et al.*, 2004), *Kinixys* spp. (Straub and Jurina, 2001), red-eared slider (*Trachemys scripta elegans*) (Straub and Jurina, 2001; Mathes *et al.*, 2010) and *Pseudemys* spp. (Mathes *et al.*, 2010). Accurate interpretation of MR images requires knowledge of normal coelomic cavity anatomy in turtles. Only two studies compared cross-sectional anatomy with MR images in loggerhead sea turtles (Valente *et al.*, 2006) and green turtles (Croft *et al.*, 2004).

The purpose of this study was to provide an atlas of the normal cross-sectional anatomy of the coelomic cavity in red-eared sliders and yellow-bellied sliders (*Trachemys scripta scripta*) using MR images and gross anatomic sections in transverse, sagittal, and dorsal planes.

Material And Methods

All procedures were approved by the Nantes National Veterinary School Animal Care and Use Committee. One adult female red-eared slider and one female and one male adult yellow-bellied slider were used in the present study. All three sliders were captive animals being group-housed in an outdoor facility at the Planète Sauvage Zoo (Port-St-Père, France). Mean body weight was 1.04 kg (2.29 lb; range 0.76–1.24 kg [1.68–2.73 lb]) and mean shell length was 18.7 cm (7.36 in; range 16.3–20.2 cm [6.42–7.95 in]).

Age was not known. Animals were considered to be healthy on the basis of a physical examination, three radiographic images (dorsoventral, right lateral, and cranio-caudal views), and plasma biochemistry evaluation (uric acid, phosphorus, calcium, albumin, total protein, alanine aminotransferase, aspartate aminotransferase, and alkaline phosphatase; ISIS, 2002).

The turtles were anesthetized with 10 mg/kg propofol (Rapinovet, Intervet/Schering-Plough Santé Animale, Beaucouze, France) in the subcarapacial vein. After intubation, anesthesia was maintained with 1% to 2% isoflurane (IsoFlu®, Isoflurane USP, Abbott Animal Health, Rungis, France). The animals were bound on a wooden board in ventral recumbency with the limbs and the head extended throughout the experiment. During image acquisition, intermittent positive-pressure ventilation was applied to the lungs to decrease motion artifacts due to respiration.

Magnetic resonance imaging was performed at the Imaging Diagnostic Service of the Veterinary Teaching Hospital of Nantes National Veterinary School with a superconducting magnet, operating at a field strength of 1 Tesla (MAGNETOM Harmony, Siemens, Erlangen, Germany), and a solenoidal human surface coil. The imaging protocol used in this study consisted of transverse, sagittal, and dorsal T1- and T2-weighted images (Table 1). No contrast medium was used.

Immediately after MR imaging, the turtles were euthanized using 0.2 mg/kg pentobarbital (Dolethal, Vetoquinol, Lure, France) in the jugular vein. The cadavers were frozen at −18°C (−0.4°F) on the wooden board in the exact same position as they had been in for the MR imaging. One turtle was sectioned in each plane (transversal, sagittal, or dorsal) in 1-cm parallel slices with an electric band saw. The cranial and caudal surfaces of each section were immediately cleaned, numbered, photographed, and replaced at −18°C (−0.4°F) for future studies. Individual anatomic structures were first labeled on photographic slides of the cadaver sections with the aid of reference anatomic textbooks (Laurence, 1962; Guibe, 1970 a, b, c; Bojanus, 1970; Wyneken, 2001; Gomis *et al.*, 2003; McArthur *et al.*, 2004; ICVGAN, 2005). Magnetic resonance images, which most closely matched each cross-sectional photograph, were chosen. Identified structures were subsequently located on selected MR images.

Results

Thirteen representative transverse combinations of images from the cranial to the caudal extremity of the shell were selected for the first turtle, 14 sagittal matched-pairs of images were chosen for the second turtle, and 11 dorsal combinations were chosen for the third turtle. Twelve selected sections are presented in a caudal-to-rostral progression. Transverse MR images and cadaver sections were oriented so that the left side of the coelom is to the viewer's right and dorsal is at the top (Figs. 1–8; Table 2), sagittal images were oriented so that the cranial part is to the viewer's left and dorsal at the top (Figs. 9–10; Table 2), and dorsal views were oriented so that the cranial part is at the top and the left side of the coelom is to the viewer's right (Figs. 11–12; Table 2).

Clinically relevant anatomic structures were identified in the MR images and anatomic cross-sectional slides. The MR images provided excellent depictions of anatomical structures when compared to their photograph. Some structures present in the cadaver sections could not be seen on the corresponding MR images and *vice versa*.

The trachea was clearly visible ventral and to the right of the esophagus on MR images. Its lumen signal intensity was hypo-intense in T1- and T2-weighted images compared to the liver and the muscles. The carina could be seen at the level of the first dorsal vertebra, as described in loggerhead sea turtles (Valente *et al.*, 2007). The left and right bronchi were best identified on their extrapulmonary course whereas their intrapulmonary course ended rapidly. The lungs were composed of two almost symmetric and non-lobed sacs, occupying the entire dorsal half of the coelom. Because of the amount of air, details of the lungs could not be recognized on MR images except for the septa (Straub and Jurina, 2001; Croft *et al.*, 2004; Valente *et al.*, 2006).

The heart was visible ventrally in the center of the cranial third of the coelom between the two hepatic lobes and adjacent to the plastron. Its shape was best observed in T2-weighted images because of the hyperintense signal of the pericardial fluid, as described in loggerhead sea turtles (Valente *et al.*, 2006). The MR signal of the myocardium was heterogeneous and slightly hyperintense to hyperintense in T1- and T2-weighted images relative to muscle. The

Table 1. Pulse sequence details of MR images.

Sequence	Repetition time (ms)	Echo time (ms)	Field of view (mm)	Matrix size	Slice thickness (mm)	Time acquisition (min:sec)
T1 sagittal	513–606	13	200 × 73	320	3	4:00
T1 dorsal	432–528	13	240 × 140	384	3	4:40
T1 transverse	467–654	13	200 × 75	320	6	3:50
T2 sagittal	3,000	76	200 × 73	320	3	3:40
T2 dorsal	3,100	75	250 × 150	448	3	4:00
T2 transverse	3,880	114	200 × 75	320	6	4:26

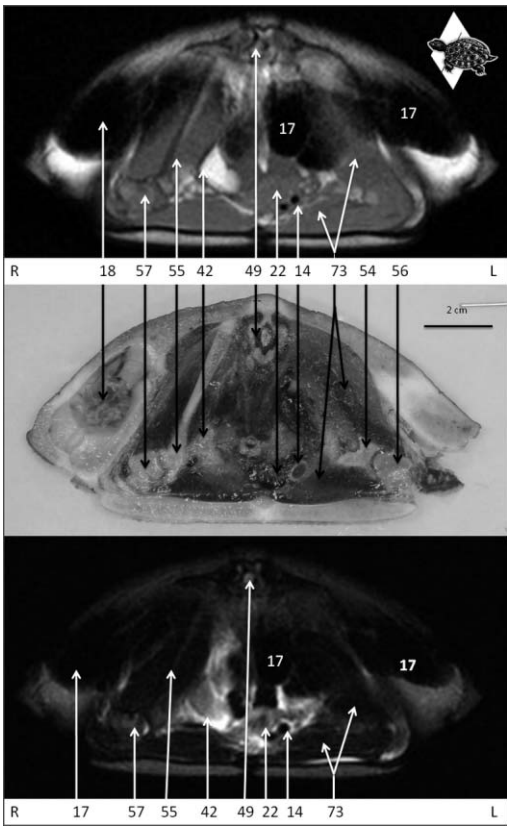

Figure 1. Transverse plane 1: T1-weighted image (top), anatomic section (middle) and T2-weighted image (below). For key see table 2.

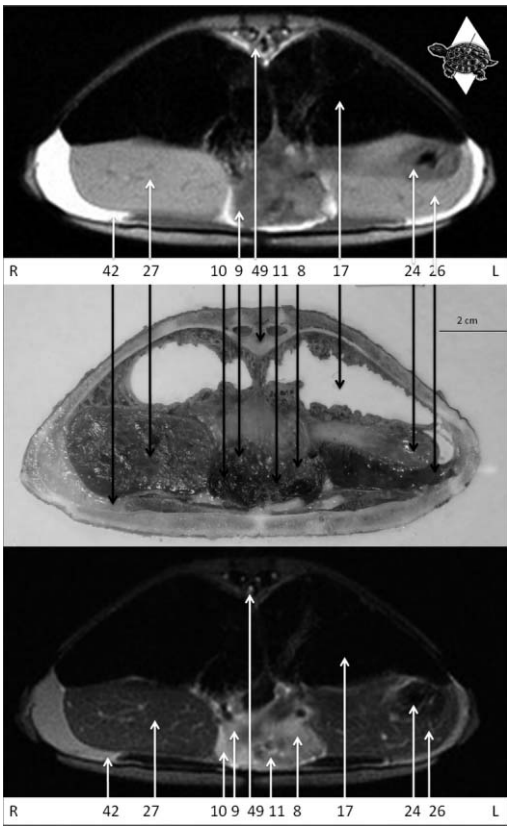

Figure 3. Transverse plane 3: T1-weighted image (top), anatomic section (middle) and T2-weighted image (below). For key see table 2.

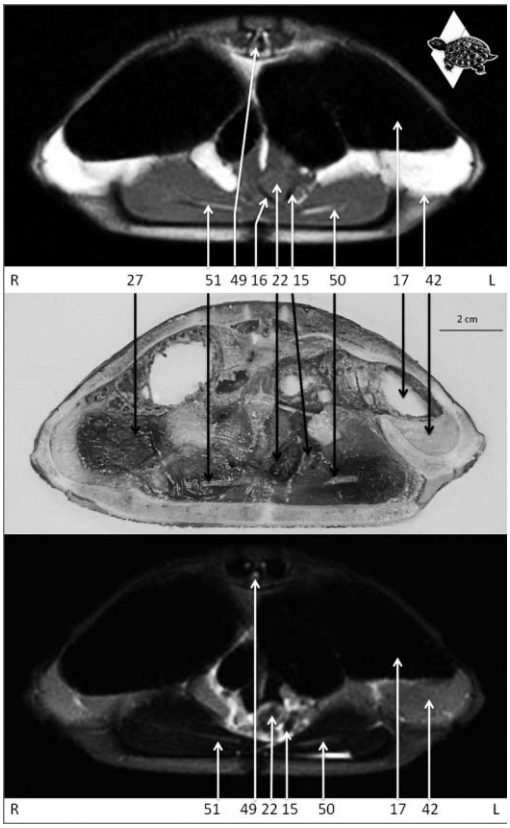

Figure 2. Transverse plane 2: T1-weighted image (top), anatomic section (middle) and T2-weighted image (below). For key see table 2.

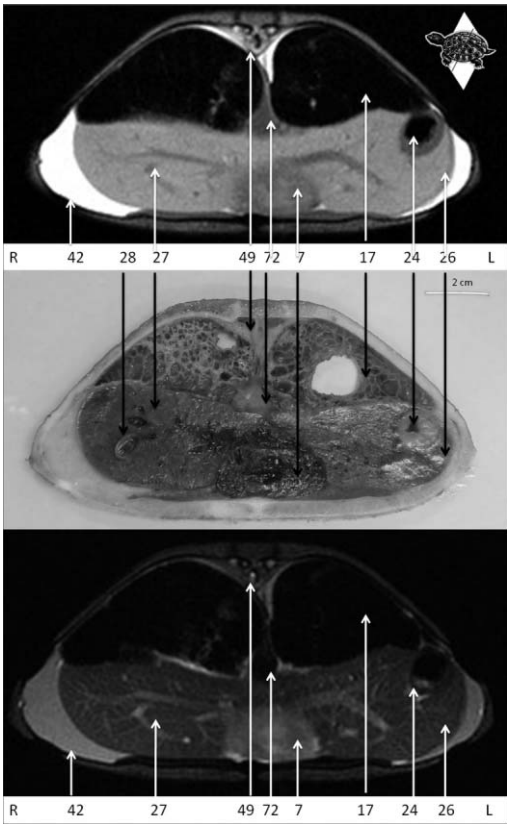

Figure 4. Transverse plane 4: T1-weighted image (top), anatomic section (middle) and T2-weighted image (below). For key see table 2.

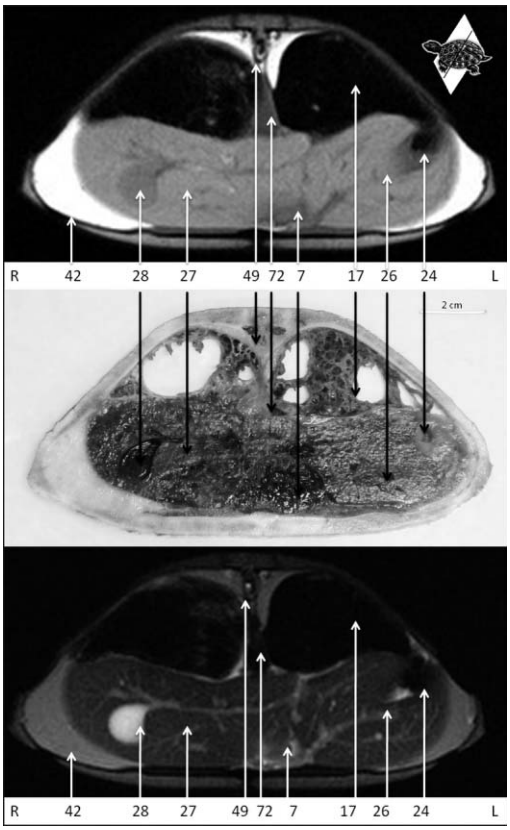

Figure 5. Transverse plane 5: T1-weighted image (top), anatomic section (middle) and T2-weighted image (below). For key see table 2.

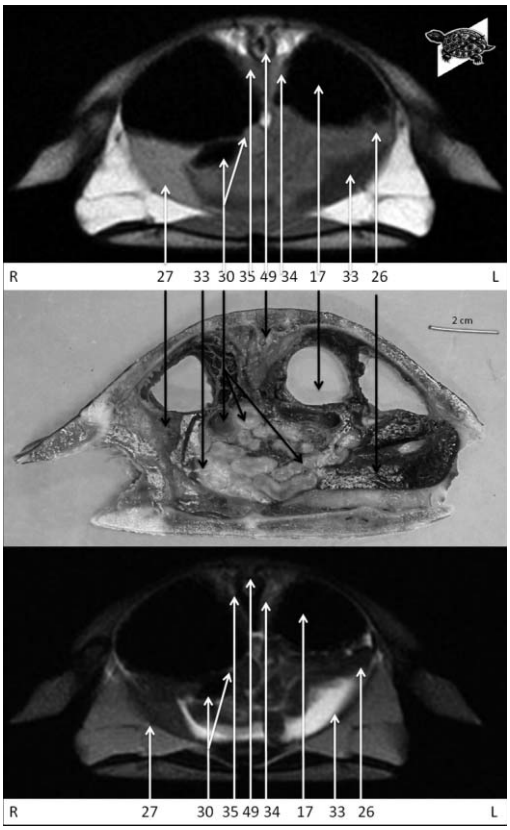

Figure 7. Transverse plane 7: T1-weighted image (top), anatomic section (middle) and T2-weighted image (below). For key see table 2.

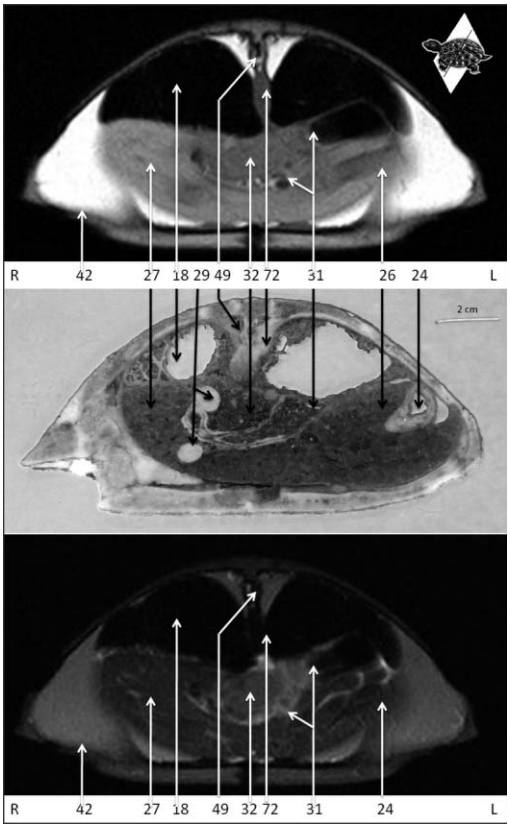

Figure 6. Transverse plane 6: T1-weighted image (top), anatomic section (middle) and T2-weighted image (below). For key see table 2.

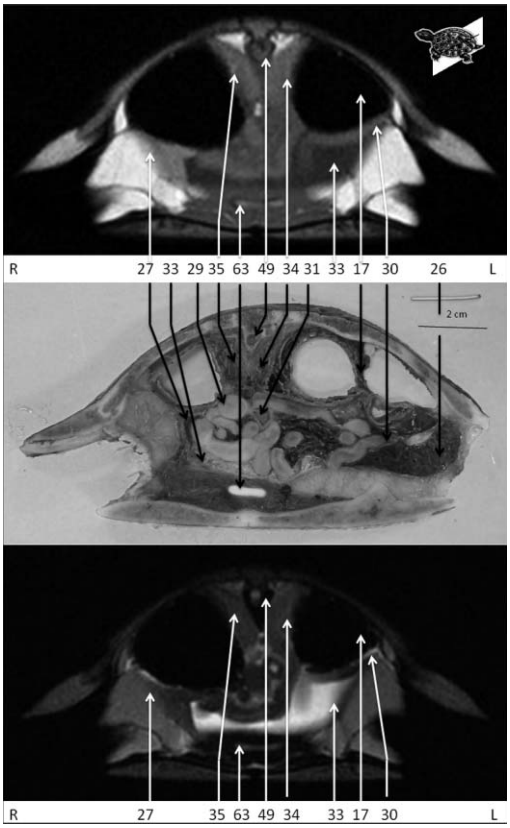

Figure 8. Transverse plane 8: T1-weighted image (top), anatomic section (middle) and T2-weighted image (below). For key see table 2.

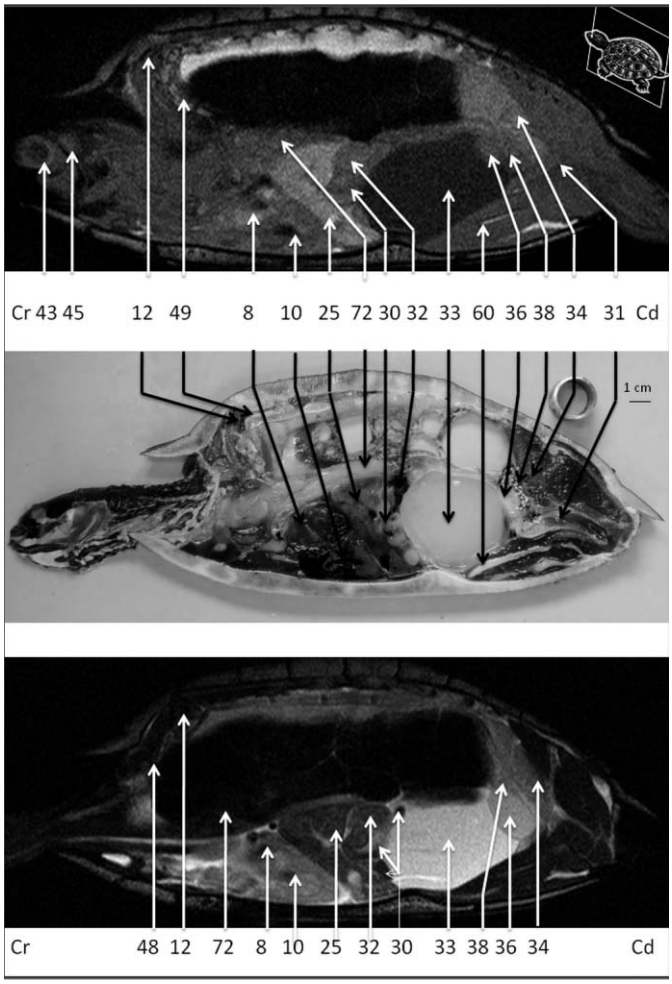

Figure 9. Sagittal plane 1: T1-weighted image (top), anatomic section (middle) and T2-weighted image (below). For key see table 2.

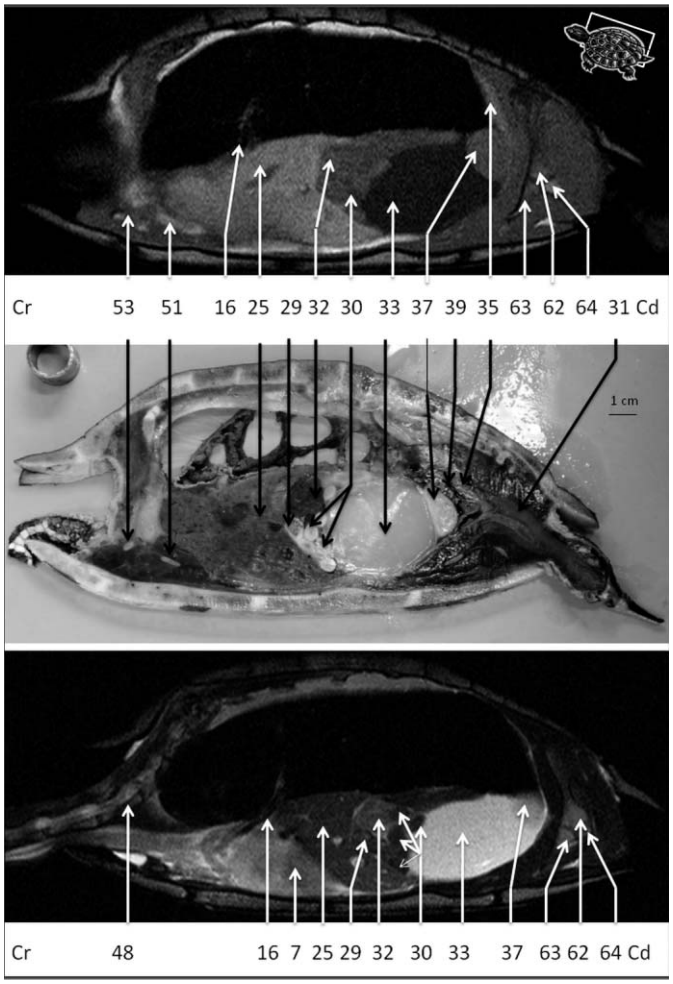

Figure 10. Sagittal plane 2: T1-weighted image (top), anatomic section (middle) and T2-weighted image (below). For key see table 2.

signal was hypo-intense in T1-weighted images and hyperintense in T2-weighted images compared to the liver. Motion artifacts caused by the heart movements could sometimes be seen on the MR images. The great vessels were identified in transverse and dorsal planes.

In all weightings, the MR signal of the digestive tract was hypo-intense compared to liver and iso-intense relative to muscle. The digestive tract lumen was easily recognized and was best seen in T2-weighted images, as digestive fluids were present. The first part of the esophagus coursed straight from the pharynx to the thoracic inlet and lay dorsal and to the left of the trachea. On dorsal images, the S-shaped curve in its caudal section was visible before the cardiac sphincter, at the level of the first dorsal vertebra. The stomach was located on the left side of the cranial half of the coelom near the left hepatic lobe, the left lung, and the carapace. The stomach had a spindle shape and greater and lesser curvatures. The duodenum coursed parallel to the caudal border of the left hepatic lobe, from the pylorus of the stomach to the gallbladder, which was located in the center of the right hepatic lobe. At this level the cranial duodenal flexure coursed caudally towards the urinary bladder. The jejunum and ileum were convoluted and occupied the median region of the second third of the coelom. The transverse colon started in the region of the cranial duodenal flexure, passed ventrally to the spleen, and terminated caudally to the stomach at the caudal border of the left hepatic lobe. At this level, after a flexure, the descending colon coursed caudally toward the pelvic inlet, passed dorsal to the urinary bladder, and terminated in the coprodeum. The ascending colon could not be identified on MR images and anatomic sections.

The liver was voluminous, bilobed, and easily recognized. It was located in the first and second third of the coelom, caudal to the heart. The right hepatic lobe was bigger than the left and extended to the reproductive tract on sagittal and dorsal planes. Relative to muscle, the MR signal of the hepatic parenchyma was hyperintense in all weightings. The gallbladder had an elliptical form and lay in the center of the right hepatic lobe. It was easily recognized in MR images as its signal was hyperintense in T2-weighted images compared to the liver and the muscles.

The spleen was an oval structure in the center of the coelom, adjacent to the cranial duodenal flexure and located caudally to the liver and ventrally to the longus colli muscle. Compared to the liver, the MR signal was hypo-intense in

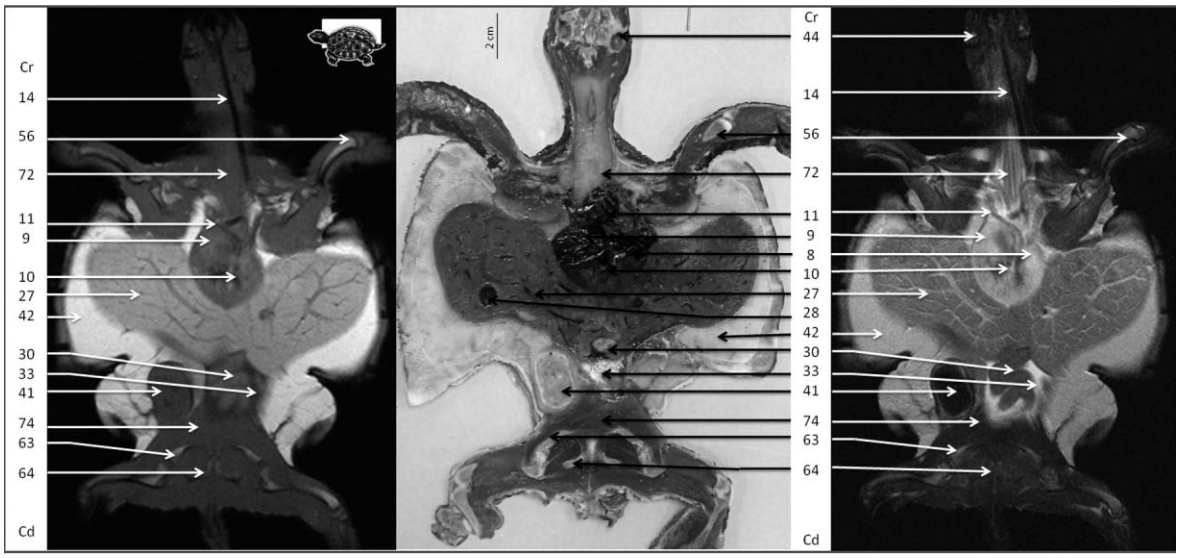

Figure 11. Dorsal plane 1: T1-weighted image (left), anatomic section (middle) and T2-weighted image (right). For key see table 2.

T1-weighted images and slightly hyperintense in T2-weighted images, as previously described (Valente *et al.*, 2006). Relative to muscle, the spleen was iso-intense and hyperintense. The pancreas was not seen on either MR series.

The kidneys had a symmetric, comma-like shape and were located dorsally between the lungs and the carapace in the last third of the coelom. Compared to the liver, the kidneys were hypo-intense in T1-weighted images and slightly hyperintense in T2-weighted images. Relative to muscle, the kidneys were hyperintense in all weightings. The ureters could not be identified. The urinary bladder was easily recognized ventrally in the last third of the coelom because of its fluid content. It was hypo-intense and hyperintense in T1- and T2-weighted images, respectively, compared to the liver and the muscles.

Some ovarian follicles and one egg were clearly visible on MR images. Ovarian follicles were small, round structures divided into layers of different intensities and located in the caudal third of the coelom. Compared to the liver, the follicles were globally iso-intense in T1-weighted images and hyperintense in T2-weighted images. Relative to muscle, the follicles were globally hyperintense in all weightings. An egg was located on the right side of the caudal third of the coelom. It was hypo-intense in all weightings compared to the liver and iso-intense and hypo-intense in T1- and T2-weighted images relative to muscle.

The male gonads could be identified on MR images and were best observed in T2-weighted images. The testicles were seen as round structures and were located ventral to the kidneys, dorsal to the distal colon, and adjacent to the (distended) urinary bladder. Each epididymis lay between

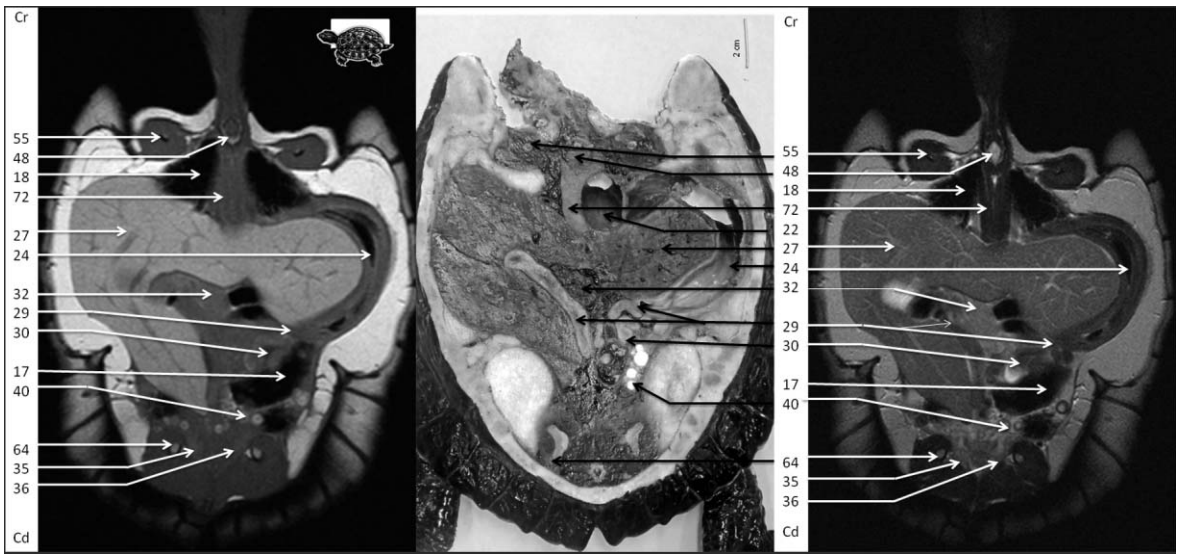

Figure 12. Dorsal plane 2: T1-weighted image (left), anatomic section (middle) and T2-weighted image (right). For key see table 2.

Table 2. Key of anatomic positions and structures for figures 1–12.

L	Left	36	Left testicle
R	Right	37	Right testicle
Cr	Cranial	38	Left epididymis
Cd	Caudal	39	Right epididymis
1	Carapace	40	Ovarian follicles
2	Plastron	41	Egg
3	Left thoracic limb	42	Fat tissue
4	Right thoracic limb	43	Left eye
5	Left pelvic limb	44	Auditory canal
6	Right pelvic limb	45	Brain
7	Heart	46	Atlas
8	Left atrium	47	Axis
9	Right atrium	48	Cervical vertebra
10	Ventricle of the heart	49	Dorsal vertebra
11	Great vessels of cardiac base	50	Left coracoid
12	Subvertebral vein	51	Right coracoid
13	Choana	52	Left acromion process
14	Trachea	53	Right acromion process
15	Left bronchus	54	Left scapula
16	Right bronchus	55	Right scapula
17	Left lung	56	Left humerus
18	Right lung	57	Right humerus
19	Pulmonary chamber	58	Pelvic symphisis
20	Longitudinal pulmonary septa	59	Left ilium
21	Pulmonary parenchyma	60	Left pubis
22	Esophagus	61	Left ischium
23	S-shaped curve of the esophagus	62	Right ilium
24	Stomach (a, cranial part; b, distal part)	63	Right pubis
25	Liver	64	Right ischium
26	Left liver lobe	65	Left femur
27	Right liver lobe	66	Right femur
28	Gallbladder	67	Left tibia
29	Duodenum	68	Right tibia
30	Small intestines	69	M. pectoralis major
31	Colon	70	M. atrahens pelvium
32	Spleen	71	M. retrahens pelvium
33	Urinary bladder	72	M. longus colli
34	Left kidney	73	Thoracic musculature
35	Right kidney	74	Pelvic musculature

Table 3. T1- and T2-weighted MR image signals of coelomic structures of red-eared and yellow-bellied sliders compared with MR image signals from liver and muscles.

	Compared with liver		Compared with muscles	
Organs–tissue	**T1-weighted**	**T2-weighted**	**T1-weighted**	**T2-weighted**
Tracheal lumen	Hypo-intense	Hypo-intense	Hypo-intense	Hypo-intense
Bronchi	Hypo-intense	Hypo-intense	Hypo-intense	Hypo-intense
Lungs	Hypo-intense	Hypo-intense	Hypo-intense	Hypo-intense
Heart	Hypo-intense	Hyperintense	Slightly hyperintense	Hyperintense
Vessels	Hypo-intense	Hyperintense	Slightly hyperintense	Hyperintense
Liver	N/A	N/A	Hyperintense	Hyperintense
Gall bladder	Hypo-intense	Hyperintense	Iso-intense	Hyperintense
Esophagus	Hypo-intense	Hypo-intense	Iso-intense	Iso-intense
Stomach	Hypo-intense	Hypo-intense	Iso-intense	Iso-intense
Duodenum	Hypo-intense	Hypo-intense	Iso-intense	Iso-intense
Intestines	Hypo-intense	Hypo-intense	Iso-intense	Iso-intense
Colon	Hypo-intense	Hypo-intense	Iso-intense	Iso-intense
Spleen	Hypo-intense	Slightly hyperintense	Iso-intense	Hyperintense
Kidney	Hypo-intense	Slightly hyperintense	Hyperintense	Hyperintense
Urinary bladder	Hypo-intense	Hyperintense	Hypo-intense	Hyperintense
Testicles	Hypo-intense	Hyperintense	Hyperintense	Hyperintense
Epididymis	Hypo-intense	Slightly hyperintense	Iso-intense	Hyperintense
Ovarian follicles	Iso-intense	Hyperintense	Hyperintense	Hyperintense
Egg	Hypo-intense	Hypo-intense	Iso-intense	Hypo-intense
Muscles	Hypo-intense	Iso-intense	N/A	N/A
Fat tissue	Hyperintense	Hyperintense	Hyperintense	Hyperintense

N/A = not applicable.

the respective testicle and kidney. Compared to liver, the testicles were hypo-intense in T1-weighted images and hyperintense in T2-weighted images. Relative to muscle, the testicles were hyperintense in T1- and T2-weighted images. The epididymides had the same MR signal as the testicles except that they were iso-intense relative to muscle in T1-weighted images. The MR signal intensities of coelomic organs in T1- and T2-weighted images compared to the liver and the muscles are synthesized in Table 3.

Discussion

T1- and T2-weighted MR images of the coelomic cavity of the red-eared and yellow-bellied sliders provide good detail of clinically relevant anatomy and correlate well with corresponding anatomic cross-sections. Transverse and sagittal planes are particularly relevant for the examination of the anatomic structures. The digestive tract is best evaluated on transverse and dorsal planes.

Using cadavers could have improved our MR image quality without the constraint of general anesthesia; however, differences in MR signals have been described between dead and live loggerhead sea turtles for vessels, parenchymatous organs (e.g., kidney and liver), and the shell (e.g., carapace and plastron) (Valente *et al*., 2006). The purpose of this study was to provide an atlas of normal MR images accessible to clinicians for diagnostic use. In order to obtain a clinically relevant atlas, we chose to use live turtles with anesthetic and acquisition protocols similar to standard procedures used in a clinical setting.

Results obtained in this study were globally similar to those from previous MR imaging studies in chelonians. Similar to the results of Valente *et al.* (2006), the authors felt that T2-weighted images provided the best details for the majority of coelomic organs except for ovarian follicles and fat tissue. However, both T1- and T2-weighted sequences should be done, as they provide complementary information for the determination of anatomic structures.

In this study it was not possible to evaluate the pulmonary structures as well as those previously described in green turtles (Croft *et al.*, 2004); this was most likely because of the small size of the sliders. However, it was possible to identify the reproductive tract of 2/3 (66%) turtles, including testicles. To the authors' knowledge, MR images of turtle testicles have not been previously reported (Straub and Jurina, 2001; Croft *et al.*, 2004; Valente *et al.*, 2006).

In T2-weighted images from the current study, the signal of the liver was hyperintense compared to the signal of the muscles. In the literature, T2-weighted liver signals have been reported as hyperintense in green turtles (Croft *et al.*, 2004) and hypo-intense in loggerhead sea turtles (Valente *et al.*, 2006). Variations in color, size, and texture of the liver have been described in chelonians related to seasons, reproductive status, metabolism during hibernation, hepatic disease, anorexia, and other pathologic conditions (McArthur *et al.*, 2004). For example, a reduction in the T2-weighted MR signal of the liver has been reported in turtles with fatty liver syndrome (Rübel *et al.*, 1994). In the previously cited studies, the green turtles suffered from cutaneous fibropapillomatosis associated with internal tumors whereas the loggerhead sea turtles were healthy, anesthetized juveniles. These differences in health status could explain the differences in liver structure and, consequently, the liver MR signals. The MR images of the three turtles from the current study were all acquired at the same time of the year (fall). Changes in liver signal could be secondary to physiological fat accumulation before hibernation. No major differences in anatomic cross-sections or MR signals relative to muscle were noted between these turtles. Further investigations should be done to evaluate the implication of physiologic and pathologic variations of the liver MR signal intensity in chelonians as well as the existence of interspecies variations.

In T2-weighted images of the turtles of this study, the myocardium had a hyperintense signal compared to the signal of muscles. Hyperintense signals in the myocardium were also observed in green turtles (Croft *et al.*, 2004), spur-thighed tortoises, and Aldabran tortoises (Wilkinson *et al.*, 2004), whereas an iso-intense signal was described in loggerhead sea turtles (Valente *et al.*, 2006). As stated previously, MR signals of the circulatory system are different between dead and live turtles because of the lack of blood flow in dead animals. However, the loggerhead sea turtles, green turtles, and sliders were all alive during the MR imaging. Caution is therefore recommended for future interpretations of MR studies regarding the chelonian circulatory system.

In this study the kidneys were hypo-intense compared to the liver in T1-weighted images. In previous studies kidney signal intensity was iso-intense compared to liver in green turtles (Croft *et al.*, 2004), Hermann's tortoises, and Greek tortoises (*Testudo graeca*) (Straub and Jurina, 2001). It has been described that hexamitiasis can increase the size and the coarseness of the kidney in MR images (Rübel and Kuoni, 1992), but to the authors' knowledge no study described changes in MR kidney signal associated with any other renal pathology or physiologic variation.

The use of MR imaging in turtle and tortoise medicine is currently limited because of its cost, availability, and the necessity of general anesthesia associated with a long acquisition time (approximately 1 h/turtle for three planes in our study). The size of the turtle could also be a limiting factor, with reduced spatial resolution and increased noise. In the current study the authors found the detail of the MR images to decrease considerably as shell length fell below 10 cm (4 in).

Computed tomography has also been described in chelonians (Rübel *et al.*, 1994; Raiti and Haramati, 1997; Gumpenberger and Henninger, 2001; Abou-Madi *et al.*, 2004; Wilkinson *et al.*, 2004; Valente *et al.*, 2007). This imaging technique shares most of the MR imaging limits (cost, availability, and general anesthesia); however, scan times are quicker and image quality is better in lungs and bone structures compared with MR imaging (Abou-Madi *et al.*, 2004). When comparing the two methods, MR imaging provides the best contrast resolution of soft tissue and allows superior evaluation of soft tissue structures (Soler *et al.*, 2007). The lower respiratory rate of turtles compared to mammals also decreases motion artifact, which can be a limiting factor in MR scan quality. Consequently, MR imaging in chelonians has a wider application field for coelomic disorders. The MR imaging application possibilities are numerous including evaluation of esophageal digestive papillae lesions secondary to foreign body ingestion in loggerhead sea turtles (Valente *et al.*, 2006), assessment of internal tumors in green turtles with cutaneous fibropapillomatosis (Croft *et al.*, 2004), and evaluation of nerve impulses (Luo *et al.*, 2009) or freeze tolerance in turtles (Rubinsky *et al.*, 1994). Even if MR imaging is not routinely used in chelonian medicine, it might become a powerful diagnostic tool to explore coelomic diseases in these animals in the near future.

In conclusion, results of this descriptive study provide a reference atlas of normal MR images of the coelomic cavity of red-eared turtles and yellow-bellied sliders that can assist clinicians with interpreting coelomic MR images. The anatomic cross-sectional photographs can also be used to facilitate location of the coelomic structures using other diagnostic techniques such as ultrasound, radiography, or computed tomography as well as to improve safety when planning a surgical approach to the coelomic cavity.

Acknowledgments: The authors would like to thank Manuel Comte for his participation in collecting the anatomical cross-sections and Dr. Delphine Féjan from the Planète Sauvage Zoo for her contribution to this study.

Literature Cited

Abou-Madi N, Scrivani PV, Kollias GV, Hernandez-Divers SN. 2004. Diagnosis of skeletal injuries in chelonians using computed tomography. J Zoo Wildl Med, 35(2):226–231.

Bojanus L. 1970. Anatome Testudinis Europae, An anatomy of the Turtle. Fascimile Reprints in Herpetology:1–178.

Croft LA, Graham JP, Schaf SA, Jacobson ER. 2004. Evaluation of magnetic resonance imaging for detection of internal tumors in green turtles with cutaneous fibropapillomatosis. J Am Vet Med Assoc, 225(9):1428–1435.

Gomis D, Deguerce C, Deguerce C, Bour R. 2003. Anatomie de la Tortue, ses Applications à la Pratique Vétérinaire. Cédérom. P. z. d. M. ENVA, Museum National d'Histoire Naturelle, Maisons-Alfort.

Guibe J. 1970a. Le squelette cephalique, le squelette du tronc et des membres, la musculature. *In* Grasse P (ed): Traité

de Zoologie. Anatomie, Systématique, Biologie: Reptiles, Caractères Généraux et Anatomie. Paris, Masson et Cie. Tome XIV, Fascicule II, 1e Partie:47–180.
Guibe J. 1970b. L'appareil circulatoire, l'appareil respiratoire, l'appareil digestif. *In*: Grasse P (ed): Traité de zoologie. Anatomie, Systématique, Biologie: Reptiles, Caractères Généraux et Anatomie. Paris, Masson et Cie. Tome XIV, Fascicule II, 2e Partie:429–548.
Guibe J. 1970c. L'appareil uro-génital. *In* Grasse P (ed): Traité de zoologie. Anatomie, Systématique, Biologie: Reptiles, Caractères Généraux et Anatomie. Paris, Masson et Cie. Tome XIV, Fascicule III:536–546.
Gumpenberger M, Henninger W. 2001. The use of computed tomography in avian and reptile medicine. Sem Avian Exotic Pet Med, 10(4):7.
[ICVGAN] International Committee on Veterinary Gross Anatomical Nomenclature. 2005. Nomina anatomica veterinaria. Hannover, Columbia, Gent, Sapporo, the Editorial Committee:1–160.
[ISIS] International Species Information System. 2002. International Species Information System Physiological Data Reference Values. CD-ROM; ISIS, Eagan, MN.
Laurence MA. 1962. Laboratory Anatomy of the Turtle. Brown Publishing, Dubuque, IA:1–48.
Luo Q, Huo L, Hanbing L, Senseman D, Worsley K, Yihong Y, Jia-Hong G. 2009. Physiologically evoked neuronal current MRI in a bloodless turtle brain: detectable or not? Neuroimage, 47(4):1268–1276.
Mathes K, Schnack M, Fehr M, editors. 2010. Computed tomography and magnetic resonance imaging: illustration of organs in *Trachemys* and *Pseudemys* spp. Proc AG ARK and ARAV, Munich, Germany, 120.
McArthur S, Meyer J, Innis C. 2004. Anatomy and physiology. *In* McArthur S, Wilkinson R, Meyer J (eds): Medicine and Surgery of Tortoises and Turtles. Blackwell Publishing Ltd., Victoria, Australia:35–72.
Raiti P, Haramati N. 1997. Magnetic resonance imaging and computerized tomography of a gravid leopard tortoise (*Geochelone pardalis pardalis*) with metabolic bone disease. J Zoo Wildl Med, 28(2):189–197.
Rübel A, Kuoni W. 1992. Die diagnose von Erkrankungen des Urogenitaltraktes von Reptilien mittels bildgebenden Verfahren (speziell MRI). *In* Tagungsbericht 4. Int Colloquium fur Pathologie und Therapie des Reptilien und Amphibien, DVG Bad Nauheim:330.
Rübel A, Kuoni W, Augustiny N. 1994. Emerging techniques: CT scan and MRI in reptile medicine. Semin Avian Exot Pet Med, 3(3):156–160.
Rubinsky B, Hong S, Storey KB. 1994. Freeze tolerance in turtles: visual analysis by microscopy and magnetic resonance imaging. Am J Physiol, 267(4 Pt 2):R1078–1088.
Silverman S, Janssen DL. 2006. *In* Mader DR (ed): Reptile Medicine and Surgery. Saunders Elsevier, Philadelphia, PA:258–264.
Soler, M., J. Murciano, Latorre R, Belda E, Agut A. 2007. Ultrasonographic, computed tomographic and magnetic resonance imaging anatomy of the normal canine stifle joint. Vet J, 174(2):351–361.
Straub J, Jurina K. 2001. Magnetic resonance imaging in chelonians. Sem Avian Exotic Pet Med, 10(4):181–186.
Valente L, Cuenca R, Zamora MA, Parga ML, Lavin S, Alegre F, Marco I. 2007. Computed tomography of the vertebral column and coelomic structures in the normal loggerhead sea turtle (*Caretta caretta*). Vet J, 174(2):362–370.
Valente L, Cuenca R, Zamora MA, Parga ML, Santiago L, Alegre F, Marco I. 2006. Sectional anatomic and magnetic resonance imaging features of coelomic structures of loggerhead sea turtles. Am J Vet Res, 67(8):1347–1353.
Wilkinson R, Hernandez-Divers S, Lafortune M, Calvert I, Gumpenberger M, McArthur S. 2004. Diagnostic imaging. *In* MacArthur S, Wilkinson R, Meyer J (ed): Medicine and Surgery of Tortoises and Turtles. Blackwell Publishing Ltd., Victoria, Australia:187–238.
Wyneken J. 2001. The Anatomy of Sea Turtles. United States Department of Commerce NOAA Technical Memorandum NMFSSEFSC-470, Miami, FL.